

RATIONAL USE OF HIGH STRENGTH CONCRETE IN FLAT SLAB– COLUMN CONNECTIONS UNDER SEISMIC LOADING

Micael Inácio, Brisid Isufi, Massimo Lapi, António Pinho Ramos

NOTE: This manuscript has been accepted for publication in *ACI Structural Journal*, Volume 117, Issue 6. This unedited manuscript will undergo copyediting, typesetting, and review of the resulting proof before it is published in its final form. The final form can be accessed through ACI's website: <https://www.concrete.org/publications/internationalconcreteabstractsportal.aspx?m=details&i=51728080>

Cite as: Inácio, M., Isufi, B., Lapi, M., & Ramos, A. P. (2020). Rational Use of High-Strength Concrete in Flat Slab-Column Connections under Seismic Loading. *Structural Journal*, 117(6), 297-310.

ABSTRACT

High Strength Concrete (HSC) slab–column connections with relatively low concrete strengths compared to today’s capabilities have been tested under seismic-type loading in the past. Herein, the hybrid use of HSC with compressive strength around 120 MPa and Normal Strength Concrete (NSC) is investigated through three reversed horizontal cyclic loading tests with different geometries of the HSC region and a reference NSC specimen. The results show that HSC applied in the vicinity of the column can significantly enhance the seismic performance of slab–column connections. The best result in terms of drift capacity and economic use of HSC was achieved in the case of full-depth HSC extended from the column’s face up to 2.5 times the effective depth. Drift ratios up to 3.0% were achieved. A comparison with previous tests showed that the hybrid use of HSC and NSC can achieve similar results to the provision of punching shear reinforcement.

Keywords: high strength concrete; punching; flat slab; cyclic loading; slab–column connection; hybrid; flat plate; seismic loading;

INTRODUCTION

Flat slabs are widespread in buildings all over the world, including in seismic areas. Given their abundance, developing solutions for an improved performance of flat slab–column connections under gravity and seismic loading is of great interest. It has been shown that one of the most efficient methods to enhance the punching shear capacity under gravity loading and the deformation capacity under horizontal loading is the provision of punching shear reinforcement^{1–6}. Besides the provision of punching shear reinforcement, successful attempts to use HSC as an alternative to enhance the punching shear strength of flat slabs under gravity loading have also been reported in the literature^{7–9}. Since the use of HSC is less labor intensive than installing punching shear reinforcement, this solution can become an attractive alternative even for seismic loading conditions if proven satisfactory.

A relatively small number of specimens with HSC have been tested under combined vertical and seismic-type horizontal loading in the past^{10–12}. Emam et al¹⁰ and Marzouk et al¹¹ reported tests on specimens that had the same overall geometry and test setup, representing the hogging moment region of isolated slab–column connections. These specimens were square, with a side dimension 1900 mm. The column’s cross section was square, with side dimension equal to 250 mm.

An enhancement of the behavior of specimens with HSC in Emam et al¹⁰ was observed compared to similar specimens with normal strength concrete. The enhancement was observed in terms of deformation capacity (and ductility) as well as strength. During the tests, the specimens with HSC were less cracked and the crack openings were smaller compared to the normal strength specimens.

The tests of Marzouk et al¹¹ indicated that high strength lightweight concrete can also be effective in enhancing the ductility and strength of slab–column connections. Specimens with HSC performed better, in that they reached a higher strength and deformation capacity compared to normal strength and normal strength lightweight concrete specimens. The enhancement in drift capacity was relatively small compared to lightweight normal strength specimens.

Seismic-type loading tests on HSC specimens were also reported in Smadi and Yasin ¹², in which the tests were conducted using a test setup and geometry (slab thickness, column dimensions etc.) very similar to that of Marzouk et al ^{10,11}, but with smaller overall dimensions (1500 mm square side). The comparison of a HSC specimen with a similar one but with NSC revealed that the ultimate rotation of the HSC specimen was significantly increased (by nearly 62%). Furthermore, the failure mode changed from flexure-punching in the specimen with NSC to flexure in the specimen with HSC.

The compressive concrete strength of the specimens tested under seismic-type loading conditions in the aforementioned publications ¹⁰⁻¹² was around 70 MPa. It is important to notice that such values of concrete strength are significantly lower than what can be achieved nowadays by the concrete industry ¹³. This is a natural consequence of the advancements in concrete production technology, which have led to an ever-increasing threshold for the designation of concrete as “high strength”. With the increase of concrete strength, however, its cost is also increased. Under these circumstances, the purpose of this paper is to study the seismic behavior of hybrid slab–column connections (i.e., with both HSC and NSC) and, starting from the promising results obtained by Inácio ¹⁴ under vertical loading conditions, to test various configurations aiming at an economization of use of HSC for seismic loading applications. To this end, the reversed horizontal cyclic loading tests of three specimens with HSC and a reference specimen with NSC are described and analyzed in detail in this paper.

For the purposes of this paper, HSC is considered a concrete without fibers (steel or any other type) into the mix. The alternative, fiber-reinforced concrete (FRC) has been used in the past to enhance the behavior of flat slab–column connections under seismic loading ^{12,15,16}.

RESEARCH SIGNIFICANCE

Slab–column connections under seismic-type loading with HSC with compressive strength around 70 MPa have been tested in the past and promising results have been obtained. To the best of the

authors' knowledge, however, the seismic behavior of slab–column connections with concrete compressive strength around 120 MPa (which is achievable nowadays) has not been previously studied experimentally. Furthermore, the economization of use of HSC is investigated in this paper for the first time for seismic-type loading, based on the promising results obtained in the past for gravity loading.

EXPERIMENTAL INVESTIGATION

Overview

The experimental campaign conducted at NOVA School of Science and Technology, Universidade Nova de Lisboa (FCT/UNL) consisted in the combined vertical and reversed horizontal cyclic loading of three flat slab specimens with HSC in the vicinity of the column. Specimen C-50, reported in Almeida et al ¹⁷, is used in this paper as a reference specimen. Compared to the specimens with HSC, specimen C-50 had the same nominal geometry, reinforcement and loading conditions, but it was made entirely of NSC. The three specimens with HSC are named CHSC1, CHSC2 and CHSC3. All four specimens (i.e., including the reference specimen C-50) had overall dimensions 4.15 m × 1.85 m and a thickness of 150 mm.

A steel HEM120 column, designed to remain elastic throughout the test, was used for convenience. The column's base plate was square with side dimension equal to 250 mm. The total height of the column (from below to above the slab) was 2 m (1 m above and below the slab). As such, the specimens represent a roughly 2/3 scaled model of a real structure.

For all the specimens, the main flexural reinforcement consisted in Ø12 top bars spaced at 100 mm in the vicinity of the column and 200 mm elsewhere (**Fig. 1**), resulting in a top flexural reinforcement ratio of 1%. Uniformly spaced (at 100 mm) Ø10 bottom bars were used (**Fig. 1**). Two bottom bars in each direction passed through the column's core, thus serving as integrity reinforcement that prevents the slab from falling on the laboratory floor in case of a punching shear failure.

HSC was applied only to a limited region near the column to rationalize its use, as illustrated in **Fig. 2**. In specimen CHSC1, the HSC was applied only to a 700 mm side square and only to the bottom 50 mm of the slab. The idea of using the HSC only in a thin layer at the bottom of the slab arose from the works of Kotsovos and Kotsovos¹⁸, Faria et al¹⁹ and Mamede et al²⁰, in which it was suggested that the compressive strength is more relevant in increasing the punching capacity than the concrete tensile strength for vertical loading conditions. Later, Inácio¹⁴ showed experimentally that for slabs subjected to monotonic vertical loading, the use of HSC only in a thin layer at the bottom of the slab provides almost the same punching strength as a slab entirely made of HSC.

In specimen CHSC2, HSC was used for the entire thickness of the slab in a square region with side dimension 1150 mm. The full thickness of the slab was filled with HSC in specimen CHSC3 as well, but the region with enhanced concrete properties was chosen smaller than in CHSC2 (850 mm square side). The main experimental variable between these three hybrid specimens was the geometry of the region with HSC.

The specimens were produced in a precast concrete facility to ensure high quality control. To ensure the desired geometry of the HSC region in accordance with **Fig. 2**, a galvanized hexagonal steel net was used as a formwork for the HSC, as shown in **Fig. 3**. The region with HSC was cast first. Soon after, the NSC part was cast. The adopted construction method proved successful in providing a finished product with monolithic connection between the two different concretes and with minimal deviations from the intended geometry.

Materials

Portland cement type CEM I 52.5R was used to produce the HSC while the NSC was produced with Portland cement CEM II/B-L 32.5N. Silica fume, in a quantity equal to 10% of the cement weight, was added to increase the mechanical proprieties of the HSC, as suggested in the literature^{21–24}. For NSC, the water cement ratio was set equal to 58% while in the HSC it was kept equal to 28%. In the HSC, superplasticizer was also added to improve the workability. For the NSC, crushed coarse limestone aggregate with fine sand were used, while crushed coarse basalt aggregates with

medium and fine sand were adopted for HSC. The maximum aggregate size was 13.9 mm for the HSC and 13.2 for the NSC.

The concrete compressive (f_c) and tensile splitting ($f_{ct,sp}$) strengths were determined on cylinders 150×300 mm, according to EN 12390-3²⁵ and EN 12390-6²⁶ respectively. The concrete modulus of elasticity (E_c) was also determined on cylinders according to EN 12390-13²⁷. Characteristics of concrete are listed in **Table 1**. The tests were performed on specimens of the same age as the respective slab.

Reinforcing steel properties were determined according to EN 10002-1²⁸ by performing direct tensile tests on bar samples. Characteristics of steel reinforcement are listed in **Table 2**, in which f_y is the yield stress, ε_y is the yield strain and E_s is the modulus of elasticity of steel.

Test setup and loading protocol

The specimens were tested using the test setup developed at FCT/UNL, which is described in detail in Almeida et al¹⁷. The edges perpendicular to the direction of loading (the short edges) of the specimens tested in this setup represent mid-span lines of a continuous flat slab frame. To ensure conditions representative of mid-span lines, the test setup allows vertical displacements at the opposite short edges and it ensures equal magnitude shear forces, bending moments and rotations at these edges. Furthermore, the setup ensures mobility of the line of inflection location along the longitudinal direction during horizontal cyclic loading. For vertical loads, the shear forces and rotations at the opposite short edges are zero and the vertical displacements and the bending moments are the same. For horizontal actions, the vertical displacements and shear forces are equal in magnitude, but with opposite signs. The test setup marks a distinction with test setups commonly used in the past, typically representing only the hogging moment region of the slab, because it enables realistic conditions with the possibility of redistribution of internal forces. The test setup is seen in action under horizontal loading conditions in **Fig. 4a, b**. A general view is given in **Fig. 4d** and photos of the setup are shown in **Fig. 5**.

To guarantee equal shear forces and vertical displacements, a passive mechanical see-saw-like system is used (**Fig. 4a**), allowing vertical displacements under gravity loading (**Fig. 4c**). When horizontal displacements take place, the system reacts by applying shear forces at the short edges to prevent the slab's rigid body rotation. The balance system ensures that those forces are equal in magnitude and opposite in direction. As the slab stiffness degrades, deformation due to the constant vertical load increases. This ensures that the vertical load is driven to the column only ²⁹.

To have positive bending moments at slab's mid-span and equal rotations at the opposite edges, a system consisting in a horizontal double pinned strut and two vertical elements is used (**Fig. 4b**). For vertical loads, a positive moment of equal magnitude is introduced at both short edges (refer to **Fig. 4c**). For horizontal action, the slab rotations are forced to be the same at the opposite edges.

The vertical load is applied through steel plates to the top slab surface in eight points to better approximate a uniformly distributed load. It is intended to be kept constant throughout the horizontal cyclic loading phase. To this end, a system of spreader beams and steel tendons as shown in **Fig. 4d** is used. This system follows the slab horizontal deformations, therefore ensuring constant gravity loads throughout the entire test. The load is applied using four hydraulic jacks connected to a Load Maintainer machine.

The loading protocol consisted in the application of the gravity load followed by imposed reversed horizontal drifts as illustrated in **Fig. 6**. The gravity load was kept constant during the application of the drifts. The concentric punching shear resistance of the specimens as if they were made entirely of NSC, V_0 , was used as a reference value to determine the magnitude of gravity loads applied in each specimen. The resistance V_0 was calculated in accordance with Eurocode 2 ³⁰, with the expression and results summarized in **Table 3**. In the calculation of V_0 , u_0 is the perimeter of the control section located at $2d$ from the face of the column, d is the effective depth, $k = 1 + \sqrt{(200/d)} \leq 2.0$, f_c is the concrete strength and ρ_1 is the geometric mean of the flexural reinforcement ratios in the two main directions. The average effective depth d was measured before casting and the values are presented in **Table 3**.

Instrumentation

Eighteen displacement transducers distributed along the two main axes of the specimen were installed to record deflections during the test, as indicated in **Fig. 7**. Another displacement transducer was installed at the level of the actuator to measure the horizontal displacements at the top of the column (drift ratios can be calculated by dividing this horizontal displacement by the total length of the column, 2 m).

Fig. 7 shows also the points in which the gravity load was applied. For each pair of gravity load application points (for each spreader beam), a load cell measured the applied load at all times. The actuator was also equipped with a load cell measuring the horizontal force. The unbalanced moment acting on the slab–column connection can be obtained by multiplying the measured force with the total length of the column.

In top bars, strain gauges were installed near the column, in eight locations in four bars, as shown in **Fig. 8** (refer also to **Fig. 1** for orientation). In each measuring location, two strain gauges were installed in diametrically opposed points.

EXPERIMENTAL RESULTS

Cracking and failure modes

The behavior of all the specimens was comparable during the gravity loading phase. Cracks parallel to the faces of the column appeared first close to the column on the top surface of the slab, followed by new parallel cracks further away from the column and radial cracks for higher levels of the gravity load. The radial cracks reached the zero moments line (i.e., edges of the specimen in the East-West direction, **Fig. 1**). Flexural cracks were also detected on the bottom surface at the sagging moment region of the specimens (at simulated mid-spans).

The first horizontal cycles were characterized by comparable cracking patterns and developments for all the specimens. It was noticed, however, that in specimens CHSC2 and CHSC3, cracks initially extended more than in CHSC1.

With the increase of drifts, the existing cracks grew in length and opening. The first to deviate from the group was specimen C-50¹⁷, which failed in a brittle punching shear mode in the second cycle with a target horizontal drift equal to 1.0%. In the following target drift level (1.5%), specimen CHSC1 failed in punching after completing two cycles. The other specimens (CHSC2 and CHSC3) continued to sustain higher drift ratios with a comparable behavior. For higher drifts, these two specimens were fully cracked, and hogging moment cracks met with the sagging moment cracks. Cracks opened and closed as a function of the direction of the applied drift in accordance with **Fig. 6**. The specimens CHSC2 and CHSC3 ultimately failed in punching, with a maximum sustained horizontal drift of 3.0%.

For all the specimens, punching failure was sudden and with little notice, except for an observed intrusion of the lower steel column stub into the slab in specimens that survived large drifts. Nonetheless, the provided integrity reinforcement was sufficient to prevent the slab from falling on the laboratory's strong floor after punching, while continuing to carry the applied gravity load.

Saw-cuts of the specimens along the longitudinal (North–South) direction are shown in **Fig. 9**. For each specimen, a complete view and a zoomed-in view in the region near the column is provided. North side is on the right of the figure for all the specimens. **Fig. 9** shows that the punching shear failure cone is not perfectly symmetric. However, a typical punching shear failure surface is observed in all the specimens. Due to the higher horizontal drift ratios at failure, the saw-cuts of specimens with HSC through the entire thickness (CHSC2 and CHSC3) reveal a higher level of damage and significantly open flexural cracks.

Force—displacement relationship

The force—displacement relationship curves are presented in **Fig. 10**. Compared to the reference specimen (C-50¹⁷), all the specimens with HSC exhibited an improved behavior. The reference specimen survived target drift ratios of only 1.0%. The application of HSC in a thin layer only at the bottom part of the slab in specimen CHSC1 led to an increased ultimate drift, equal to 1.5% (**Fig.**

10b). However, the capacity enhancement was more pronounced when the entire depth of the slab was cast with HSC, as in case of specimens CHSC2 and CHSC3 (**Fig. 10c, d**).

Fig. 10 indicates that the maximum unbalanced moment transfer capacity (governed by flexure) of the slab–column connections was reached in specimens CHSC2 and CHSC3, in which drifts from 2.0% to 3.0% were characterized by a small variation of the horizontal load. On the contrary, failure occurred in specimens C-50 and CHSC1 while the horizontal load was still exhibiting an increasing trend.

Table 4 summarizes the main experimental results, including the maximum horizontal force, (H_{max}), horizontal displacement at maximum force (Δ_m) as well as the ultimate drifts ($d_{r,u}$). **Table 4** confirms that specimens CHSC2 and CHSC3 indeed behaved very similarly, with comparable maximum loads, displacements for maximum load and ultimate drift capacity. Referring to the extent of the zone with HSC (refer to **Fig. 2**), the results indicate that the geometry used in CHSC3 is sufficient, because increasing the region cast with HSC in CHSC2 did not lead to any notable improvement.

A further comparison of the specimens can be made by referring to **Fig. 11**, which shows that the initial stiffness of all the specimens was comparable. Specimen CHSC1 continued to closely follow the group of specimens with HSC but failed earlier than the other two. The plastic region of the enveloping curves (i.e., for drift larger than around 2.0%) was similar for both specimen CHSC2 and CHSC3, but the horizontal load was slightly lower in the former.

Although the solution with HSC applied over a limited depth of the specimen exhibited good performance under gravity loading ¹⁴, the same cannot be said for seismic-type loading. Specimen CHSC1 that had HSC only in the bottom 50 mm did not exhaust the entire unbalanced moment transfer capacity and failed before reaching the horizontal plateau observed in the other two specimens with HSC. A likely explanation for this observed behavior is that cyclic loading enforces sign reversal of the moment acting in the slab–column connection, resulting in the presence of

alternated tensile and compressive local stresses in the upper layers of the slab that render the application of HSC on only the bottom part insufficient.

Equivalent viscous damping

Based on the force—displacement relationships for each specimen (**Fig. 10**), an equivalent viscous damping ratio, ζ_{eq} , is calculated for each complete cycle as follows ³¹:

$$\zeta_{eq} = \frac{1}{4\pi} \left(\frac{E_{d1}}{E_{S1}} + \frac{E_{d2}}{E_{S2}} \right) \quad (1)$$

where E_d is the dissipated energy (area enclosed by the hysteresis loop) and E_s is the elastic strain energy (considering secant stiffness up to the maximum drift for each cycle), with the subscript 1 referring to positive cycles and subscript 2 for negative cycles. The results are plotted in **Fig. 12**.

Fig. 12 shows that there is a tendency to have increasing ζ_{eq} with the increment of drifts. This is a natural consequence of the increase of damage in the specimens with the increment of drifts. Referring to cycles with the same target drift, it is noticed that the first cycle is the one with a higher equivalent viscous damping. This indicates that the majority of damage can be attributed to the magnitude of the drift rather than to the number of repetitions of low-drift cycles. Comparing the specimens in **Fig. 12**, it is concluded that the differences are relatively small from specimen to specimen up to failure.

Strength and stiffness degradation

Strength degradation due to repeated cyclic loading can be observed in the envelope curves of **Fig. 11** as well as the force – displacement curves of **Fig. 10**. The vertical drops in **Fig. 11** represent strength degradation due to repeated loading. The last drop represents failure. The strength degradation increased progressively with the increase of the drifts. For the specimens that reached a horizontal plateau in the force – displacement relationship (i.e. specimens CHSC2 and CHSC3), the degradation of strength from the first to the third cycle within the same target drift was approximately 10% after global yielding. For lower drifts the in-cycle degradation was lower, and comparable with that of the other two specimens (C-50 and CHSC1) for the respective drifts.

Fig. 13 shows the secant stiffness of all the specimens as a function of the target drift ratio. Two types of degradations can be distinguished in the figure: a degradation with the increase of the drifts and a degradation for repeated loading, marked by the steps in the graph. At target drift ratio equal to 1.0%, the reference specimen started to deviate from the other specimens, as already observed from **Fig. 11**. This is also reflected in the secant stiffness in **Fig. 13**, where the values for C-50 are lower than those for the specimens with HSC at 1% drift. The evolution of stiffness with the increase of drifts was almost identical in the two specimens with HSC over the entire depth (CHSC2 and CHSC3), even though the extent of the HSC region was different. Note that the graphs are slightly shifted along the horizontal axis to improve readability.

Deflections

Deflection profiles were extracted from the readings of the displacement transducers installed on top of the specimen (**Fig. 7**). The results for the longitudinal direction are shown in **Fig. 14** for an application of the horizontal load directed towards South. The figures are similar (symmetrical) for a reversed direction of loading. The deflection profiles in **Fig. 14** correspond to peak drifts of the loading history of **Fig. 6**. For each target drift level, only the results for the first and third cycle are shown.

Fig. 14 demonstrates that the deflections after the application of the gravity load were comparable in all specimens. The application of horizontal drifts led to an increase of the deflections due to the degradation of the stiffness of the slab. Comparable deflections for the same drift were observed in all the specimens regardless of the geometry of the HSC region. The differences became apparent only for large drifts, where CHSC3 deformed slightly more than CHSC2. Referring to the deflection profiles corresponding to the same target drift ratio, it is observed that cycle repetitions caused an increase of deflections. This increase of deflections shows the detrimental effect of lateral cyclic loading on the bending stiffness of the slab.

The deflection profiles of **Fig. 14** indicate also that the test setup worked as intended. It ensured equal deflections and rotations at mid-span locations and it provided the conditions of a continuous

flat slab, i.e., with both hogging and sagging bending moment regions. To further analyze the deflection profiles, the location of the inflection point throughout the test was estimated by fitting the displacement transducer data into polynomial functions. The results are presented in **Fig. 15**, where it is noticed that the inflection point was not fixed throughout the horizontal cyclic loading test. At the end of the gravity loading phase it was close to the theoretical value of 22% of the span (actual values in **Fig. 15** are slightly larger, around 25% of the span). The location of the inflection point follows the direction of the applied horizontal drifts. For the two specimens that reached high drift ratios (CHSC2 and CHSC3), the inflection point reached the column, indicating the presence of sagging bending moments in the slab in the vicinity of the column. When the inflection point shifts towards mid-span, it does not surpass 28% of the span.

Longitudinal reinforcement strains

For strain gauge readings of specimen C-50, the reader is referred to Almeida et al ¹⁷, where it was shown that the bar closest to the column started to yield for relatively low drifts, whereas the strain in the other instrumented bars was well below yielding limit when punching shear failure occurred. For the specimens with HSC, the strain gauge readings are presented in **Fig. 16**. The strains in **Fig. 16** are shown only for the first excursion in each drift level of the loading history of **Fig. 6**. Also, strains in **Fig. 16** are shown only for the side of the slab under hogging moments due to the imposed unbalanced moment. Strains on the symmetrical locations were always lower than the ones shown in the figure. The strain values in **Fig. 16** are obtained as the average of the two readings from the strain gauges installed in each measurement location (**Fig. 8**). The measurement locations are referenced in **Fig. 16** using B (which stands for “bar”) followed by the bar number (counting starts from the center of the slab) and the side on which the strain gauges are installed (N or S). For example, location B5N refers to strain gauges installed on the north side of the slab at the fifth bar, i.e. strain gauges 11 and 12 in **Fig. 8**.

No yielding was detected during the gravity loading phase. The magnitude of strains at the end of gravity loading phase does not appear to be related to the geometry of the HSC region. In specimen

CHSC3, the strain in the bar closest to the column was close to yielding. **Fig. 16** shows that strains increase with the increase of lateral drifts, with bars closer to the column having higher strains. Strain distribution becomes non-symmetrical for horizontal loading due to the acting unbalanced moment in the slab–column connection. In specimens CHSC1 and CHSC3, yielding was detected in all instrumented bars. In specimen CHSC2, yielding was detected in the bar closest to the column but for the rest of the bars the strain gauges stopped working before recording yielding strains. Given the similar behavior of CHSC2 with CHSC3, it is reasonable to expect that yielding of all the instrumented bars has occurred in CHSC2 as well. The results are generally in agreement with observations from the load – displacement curves (**Fig. 10**).

COMPARISON OF USING HSC WITH OTHER SEISMIC PERFORMANCE ENHANCEMENT TECHNIQUES

A series of experiments conducted using the test setup of **Fig. 4** have been published recently. Gouveia et al ³² reported four reversed horizontal cyclic loading tests of specimens with steel fiber-reinforced concrete (SFRC) in the vicinity of the column. The specimens differed by the fiber content and type. Isufi et al ⁴ reported the tests conducted on five specimens, four of which contained headed shear stud reinforcement. The main variables in Isufi et al ⁴ were the extent of the shear-reinforced zone and the magnitude of the gravity load. Almeida et al ⁵ described the tests conducted on four specimens with stirrups, with varying amount of punching shear reinforcement and varying extent of the shear-reinforced zone. Post-installed bolts were tested as a strengthening solution in Almeida et al ⁶.

Besides being tested on the same test setup, all the aforementioned specimens had the same nominal geometry as well as flexural reinforcement. Furthermore, many of the specimens had comparable applied vertical loads. **Table 5** summarizes the main characteristics of a subset of such specimens, chosen on the basis of the magnitude of the applied vertical load. The table contains the name of the specimen, the method used to enhance its performance, the extent of the zone in which the

enhancement method is applied, the vertical load V_g , the maximum unbalanced moment M_{max} and the ultimate drift $d_{r,u}$. Besides the small differences from specimen to specimen in the applied load, V_g , the ratio between V_g and the concentric punching shear resistance V_0 was approximately the same for all the specimens presented in the table (V_g/V_0 about 50%). As a consequence, concrete strengths of specimens with approximately the same V_g were close to each other.

Table 5 shows that the performance of the specimens with HSC in the entire depth (specimens CHSC2 and CHSC3) was comparable with that of similar specimens with conventional punching shear reinforcement in terms of maximum unbalanced moment and ultimate drift ratio. For instance, comparing CHSC2 with C-50 STR3 with stirrups, it is noticed that the ultimate drift capacity of these two specimens with almost the same value of V_g was the same. C-50 STR3 had a low amount of punching shear reinforcement. Other similar specimens, but with a higher amount of punching shear reinforcement resisted higher drifts (C-SSR3 with studs and C-50 STR4 with stirrups).

Specimen CHSC3, which had a higher V_g compared to CHSC2, can be compared to C-SSR5b with studs and C-50 STR1 and C-50 STR2 with stirrups. The same observation is made: the drift capacity of the HSC specimen was comparable with that of a specimen with a low amount of punching shear reinforcement (in this case, the drift capacity of CHSC3 was slightly higher than that of the comparable specimen with a low amount of punching shear reinforcement, C-50 STR1). Again, when the amount of punching shear reinforcement is increased, the drift capacity of the shear-reinforced specimens exceeds that of the HSC specimen, or it is the same as in case of C-50 STR2. Nonetheless, in both cases (CHSC2 and CHSC3), the unbalanced moment transfer capacity (M_{max}) of the slab–column connection was comparable with the other specimens of **Table 5** that reached a horizontal plateau in the force–displacement relationship. In seismic loading conditions, this indicates that the use of HSC in a limited region near the column has the advantage of increasing the punching shear capacity without significantly modifying the flexural behavior of the slab–column connection. The result is a ductile behavior similar to what is achieved by employing a sufficient amount of punching shear reinforcement.

Comparing the HSC specimens with SFRC ones in **Table 5**, it is noticed that higher drift capacities were achieved in the specimens with SFRC, except for the case of the specimen with the lowest amount of fibers, F0.5_4D, in which the ultimate drift capacity was the same (3.0%). **Table 5** shows also that the maximum unbalanced moment is higher in specimens with a higher amount of fibers compared to all the other specimens, including those with HSC.

CONCLUSIONS

An experimental program consisting in the reversed horizontal cyclic loading test of three specimens with HSC applied in the vicinity of the column was presented in this paper. The only experimental variable was the geometry of the HSC region, aiming at economically feasible solutions for practical use. The main conclusions are listed below:

- The performance of the specimens with HSC in the vicinity of the column was enhanced compared to the reference specimen (made entirely of NSC). The drift capacity of the specimens with HSC was increased 1.5 to 3.0 times compared to the reference specimen.
- Although very promising results were obtained in a previous experimental program during the concentric monotonic test of a specimen with HSC applied only in the bottom 50 mm of the slab in the vicinity of the column, the behavior of a similar specimen (CHSC1) under horizontal loading was not nearly as satisfactory. The ultimate drift was increased (from 1.0% in the reference specimen to 1.5% in CHSC1), but the other specimens with a full depth HSC region performed significantly better. The likely explanation for the small increase in the drift capacity compared to the reference specimen is sign reversal of stresses during cyclic loading. An economization of the HSC material by applying it in a limited depth of the slab is therefore not recommended for seismic loading conditions until further verification.
- Specimens with a full depth HSC region were able to exhaust the full unbalanced moment transfer capacity of the slab–column connection, leading to a significantly improved

behavior (drifts up to 3.0%) and a more ductile response compared to the reference specimen and specimen CHSC1.

- The behavior of the two specimens with a full depth HSC region but with different size (CHSC2 and CHSC3) was very similar in all aspects (strength, deformation capacity, energy dissipation etc.). This indicates that an economization of the HSC material can be sought in terms of limiting the size in plan of the HSC region. The smaller region applied in CHSC3 was sufficient in providing a more ductile behavior and a significant drift capacity enhancement compared to the reference specimen.
- Comparing the behavior of the HSC specimens presented in this paper with previously published specimens with SFRC, studs and stirrups, it was shown that the application of HSC in the flat slab in the vicinity of the column can have similar effects to the application of conventional punching shear reinforcement or low amounts of fibers into SFRC.

Further research on the seismic behavior of slab – column connections with HSC is recommended. The presented tests can form the basis for further experimental tests and numerical analyses aiming at the development of analytical procedures applicable to general cases. Issues to be addressed include the influence of slab thickness, gravity load and flexural reinforcement ratio in the optimum geometry of the HSC region.

ACKNOWLEDGEMENTS

This work received support from the Fundação para a Ciência e Tecnologia – Ministério da Ciência, Tecnologia e Ensino Superior through projects EXPL/ECM – EST/1371/2013 and PTDC/ECI-EST/30511/2017 and scholarship number SFRH/BD/76242/2011. The authors are grateful to Concremat for making the specimens, CIMPOR for providing the cement and Sika for providing VISCOCRETE 20HE and SIKACRETE HD.

REFERENCES

1. Broms, C. E. “Flat Plates in Seismic Areas: Comparison of Shear Reinforcement Systems,” *ACI Structural Journal*, V. 104, No. 6, 2007, pp. 712–21.
2. Lips, S., Ruiz, M. F., and Muttoni, A. “Experimental Investigation on Punching Strength and Deformation Capacity of Shear-Reinforced Slabs,” *ACI Structural Journal*, V. 109, No. 6, 2012, pp. 889–900.
3. Ferreira, M. P., Melo, G. S., Regan, P. E., et al. “Punching of reinforced concrete flat slabs with double-headed shear reinforcement,” *ACI Structural Journal*, V. 111, No. 2, 2014, pp. 363–74.
4. Isufi, B., Pinho Ramos, A., and Lúcio, V. “Reversed horizontal cyclic loading tests of flat slab specimens with studs as shear reinforcement,” *Structural Concrete*, V. 20, No. 1, 2019, pp. 330–47.
5. Almeida, A. F. O., Alcobia, B., Ornelas, M., et al. “Behaviour of reinforced-concrete flat slabs with stirrups under reversed horizontal cyclic loading,” *Magazine of Concrete Research*, V. 72, No. 7, 2020, pp. 339–56.
6. Almeida, A. F. O., Ramos, A. P., Lúcio, V., et al. “Behavior of RC flat slabs with shear bolts under reversed horizontal cyclic loading,” *Structural Concrete*, V. 21, No. 2, 2020, pp. 501–16.
7. Marzouk, H., and Hussein, A. “Experimental investigation on the behaviour of high-strength concrete slabs,” *ACI Structural Journal*, No. September-october, 1991, pp. 701–13.
8. Ozden, S., Ersoy, U., and Ozturan, T. “Punching shear tests of normal- and high-strength concrete flat plates,” *Canadian Journal of Civil Engineering*, V. 33, No. 11, 2006, pp. 1389–400.
9. Inácio, M. M. G., Almeida, A. F. O., Faria, D. M. V., et al. “Punching of high strength concrete flat slabs without shear reinforcement,” *Engineering Structures*, V. 103, 2015, pp. 275–84.

10. Emam, M., Marzouk, H., and Hilal, M. S. "Seismic response of slab-column connections constructed with high-strength concrete," *ACI Structural Journal*, V. 94, No. 2, 1997, pp. 197–205.
11. Marzouk, H., Osman, M., and Hussein, A. "Cyclic Loading of High-Strength Lightweight Concrete Slabs," No. 98, 2001, pp. 207–14.
12. Smadi, M. M., and Bani Yasin, I. S. "Behavior of high-strength fibrous concrete slab-column connections under gravity and lateral loads," *Construction and Building Materials*, V. 22, No. 8, 2008, pp. 1863–73.
13. Aitcin, P.-C. "High Performance Concrete: modern concrete technology 5," New York, CRC press, 2004, 624 pp.
14. Inácio, M. M. G., Lapi, M., and Pinho Ramos, A. "Punching of reinforced concrete flat slabs – Rational use of high strength concrete," *Engineering Structures*, V. 206, 2020, p. 110194.
15. Cheng, M.-Y., and Parra-Montesinos, G. J. "Evaluation of Steel Fiber Reinforcement for Punching Shear Resistance in Slab-Column Connections - Part I: Monotonically Increased Load," *ACI Structural Journal*, V. 107, No. 01, 2010, pp. 101–9.
16. Gouveia, N. D., Faria, D. M. V., and Ramos, A. P. "Assessment of SFRC flat slab punching behaviour – part I: monotonic vertical loading," *Magazine of Concrete Research*, V. 71, No. 11, 2019, pp. 587–98.
17. Almeida, A. F. O., Inácio, M. M. G., Lúcio, V. J. G., et al. "Punching behaviour of RC flat slabs under reversed horizontal cyclic loading," *Engineering Structures*, V. 117, 2016, pp. 204–19.
18. Kotsovos, G. M., and Kotsovos, M. D. "Flat slabs without shear reinforcement: Criteria for punching," *Structural Engineer*, V. 87, No. 1, 2009, pp. 2–8.
19. Faria, D. M. V., Biscaia, H., Lucio, V. J. G., et al. "Material and Geometrical Parameters Affecting Punching of Reinforced Concrete Flat Slabs." fib Symposium 2011 - Concrete Engineering for Excellence and Efficiency. Prague, 2011.

20. Silva Mamede, N. F., Pinho Ramos, A., and Faria, D. M. V. “Experimental and parametric 3D nonlinear finite element analysis on punching of flat slabs with orthogonal reinforcement,” *Engineering Structures*, V. 48, 2013, pp. 442–57.
21. Duval, R., and Kadri, E. H. “Influence of silica fume on the workability and the compressive strength of high-performance concretes,” *Cement and Concrete Research*, V. 28, No. 4, 1998, pp. 533–47.
22. Igarashi, S. I., Watanabe, A., and Kawamura, M. “Evaluation of capillary pore size characteristics in high-strength concrete at early ages,” *Cement and Concrete Research*, V. 35, No. 3, 2005, pp. 513–9.
23. Bhanja, S., and Sengupta, B. “Influence of silica fume on the tensile strength of concrete,” *Cement and Concrete Research*, V. 35, No. 4, 2005, pp. 743–7.
24. Siddique, R. “Utilization of silica fume in concrete: Review of hardened properties,” *Resources, Conservation and Recycling*, V. 55, No. 11, 2011, pp. 923–32.
25. CEN. “EN 12390-3 Testing hardened concrete Part 3: Compressive strength of test specimens,” Bruxelles, 2001, 15 pp.
26. CEN. “EN 12390-6 Testing hardened concrete Part 6: Tensile splitting strength of test specimens,” Bruxelles, 2000, 10 pp.
27. CEN. “EN 12390-13 Testing hardened concrete Part 13: Determination of secant modulus of elasticity in compression,” Bruxelles, 2013, 16 pp.
28. CEN. “EN 10002-1 Metallic materials Tensile testing Part 1: method of test at ambient temperature,” Bruxelles, 2001, 57 pp.
29. Ramos, A., Marreiros, R., Almeida, A., et al. “Punching of flat slabs under reversed horizontal cyclic loading.” In: Ospina, C. E., Mitchell, D., Muttoni, A., eds. *ACI Special Publication*, vol. 315. ACI, fib, 2017. pp. 253–72.
30. CEN. “EN 1992-1-1. Eurocode 2 — Design of concrete structures. Part 1-1: General rules and rules for buildings,” 2004.

31. Hose, Y. D., and Seible, F. "Performance Evaluation Database for Concrete Bridge Components and Systems under Simulated Seismic Loading. PEER Report No. 1999/11," San Diego, California, 1999, 114 pp.
32. Gouveia, N. D., Faria, D. M. V., and Ramos, A. P. "Assessment of SFRC flat slab punching behaviour – part II: reversed horizontal cyclic loading," *Magazine of Concrete Research*, V. 71, No. 1, 2019, pp. 26–42.

TABLES AND FIGURES

List of tables:

Table 1—Mechanical proprieties of concrete

Table 2—Mechanical proprieties of steel reinforcement

Table 3—Gravity load in each specimen

Table 4—Summary of main test results

Table 5—Summary of main characteristics of comparable specimens tested at FCT/UNL

List of figures:

Fig. 1—Overall geometry and reinforcement of the specimens (units: mm).

Fig. 2—Geometry of the HSC region in specimens (units: mm).

Fig. 3—Production of the specimens.

Fig. 4—Test setup; a) vertical displacement and shear force compatibilization system under slab's vertical and horizontal deformation; b) rotation and bending moment compatibilization system under slab's vertical and horizontal deformation; c) bending moments diagram under gravity loading; d) general view.

Fig. 5—Photos of the test setup.

Fig. 6—Horizontal loading protocol.

Fig. 7—Instrumentation and gravity load application points.

Fig. 8—Instrumentation of top flexural reinforcement bars.

Fig. 9—Saw-cuts of the specimens.

Fig. 10—Force—displacement relationship for specimen: a) C-50; b) CHSC1; c) CHSC2 and d) CHSC3.

Fig. 11—Envelope force—displacement curves for all specimens.

Fig. 12—Equivalent viscous damping; a) C-50; b) CHSC1; c) CHSC2; d) CHSC3.

Fig. 13–Stiffness degradation

Fig. 14–Deflection profiles in the longitudinal (North-South) direction.

Fig. 15–Location of the inflection point in the longitudinal direction of the specimens; a) C-50; b) CHSC1; c) CHSC2; d) CHSC3.

Fig. 16–Strain gauge readings in the flexural reinforcement; a) CHSC1; b) CHSC2; c) CHSC3.

Table 1–Mechanical proprieties of concrete

Specimen	NSC			HSC		
	f_c (MPa)	$f_{ct,sp}$ (MPa)	E_c (MPa)	f_c (MPa)	$f_{ct,sp}$ (MPa)	E_c (MPa)
C50*	52.4	2.9	-	-	-	-
CHSC1	61.6	4.1	35700	115.2	7.1	53700
CHSC2	45.9	3.5	37300	120.2	7.4	51400
CHSC3	48.9	-**	35300	123.6	8.2	52800

*Specimens investigated by Almeida et al. ¹⁷. ** Not available.

Table 2–Mechanical proprieties of steel reinforcement

Reinforcement					
f_y (MPa)		ϵ_y (‰)		E_s (GPa)	
Ø10	Ø12	Ø10	Ø12	Ø10	Ø12
535	526	2.7	2.6	198	200

Table 3–Gravity load in each specimen

Specimen	d (mm)	$V_0 = u_0 d 0.18k(100\rho_f f_c)^{1/3}$ (kN)	V_g (kN)	V_g/V_0 (%)
C-50 ¹⁷	118.4	391.0	203.4	52.0
CHSC1	118.1	411.3	221.6	53.9
CHSC2	117.5	370.5	199.7	53.9

CHSC3	118.4	382.1	212.9	55.7
-------	-------	-------	-------	------

Table 4–Summary of main test results

Specimen	V_g (kN)	H_{max} (kN)		Δ_m (mm)		$d_{r,u}$ (%)
		South	North	South	North	
C-50 ¹⁷	203.4	37.4	-36.7	21.5	-20.0	1.0%
CHSC1	221.6	52.3	-49	30.3	-30.0	1.5%
CHSC2	199.7	55.8	-54.4	49.8	-50.0	3.0%
CHSC3	212.9	58.4	-56.7	49.9	-50.1	3.0%

Table 5–Summary of main characteristics of comparable specimens tested at FCT/UNL

Specimen	Performance enhancement method	Extent*	V_g (kN)	M_{max} (kNm)	$d_{r,u}$ (%)
CHSC1	HSC, 1/3 of slab depth	$1.9d$	222	104.6	1.5
CHSC2	HSC, entire depth	$3.8d$	200	111.6	3.0
CHSC3	HSC, entire depth	$2.5d$	213	116.8	3.0
F0.5_4D ³²	SFRC, 0.5% vol., type 4D	$2.8d$	196	119.0	3.0
F0.75_4D ³²	SFRC, 0.75% vol., type 4D	$2.8d$	194	145.4	5.5
F1.0_4D ³²	SFRC, 1.0% vol., type 4D	$2.8d$	208	133.3	>6.0
C-SSR3 ⁴	Studs, 12Ø8 per perimeter	$1.5d$	196	120.8	4.0
C-SSR5b ⁴	Studs, 12Ø8 per perimeter	$2.7d$	214	117.8	5.5
C-50 STR1 ⁵	Stirrups, 16Ø4.5 per perimeter	$1.5d$	210	99.0	2.5
C-50 STR2 ⁵	Stirrups, 8Ø6+8Ø8 per perimeter	$1.5d$	216	104.0	3.0
C-50 STR3 ⁵	Stirrups, 16Ø4.5 per perimeter	$2.7d$	202	118.6	3.0

C-50 STR4 ⁵	Stirrups, 8Ø6+8Ø8 per perimeter	2.7d	196	116.8	4.0
------------------------	---------------------------------	------	-----	-------	-----

* rounded value, measured from the face of the column

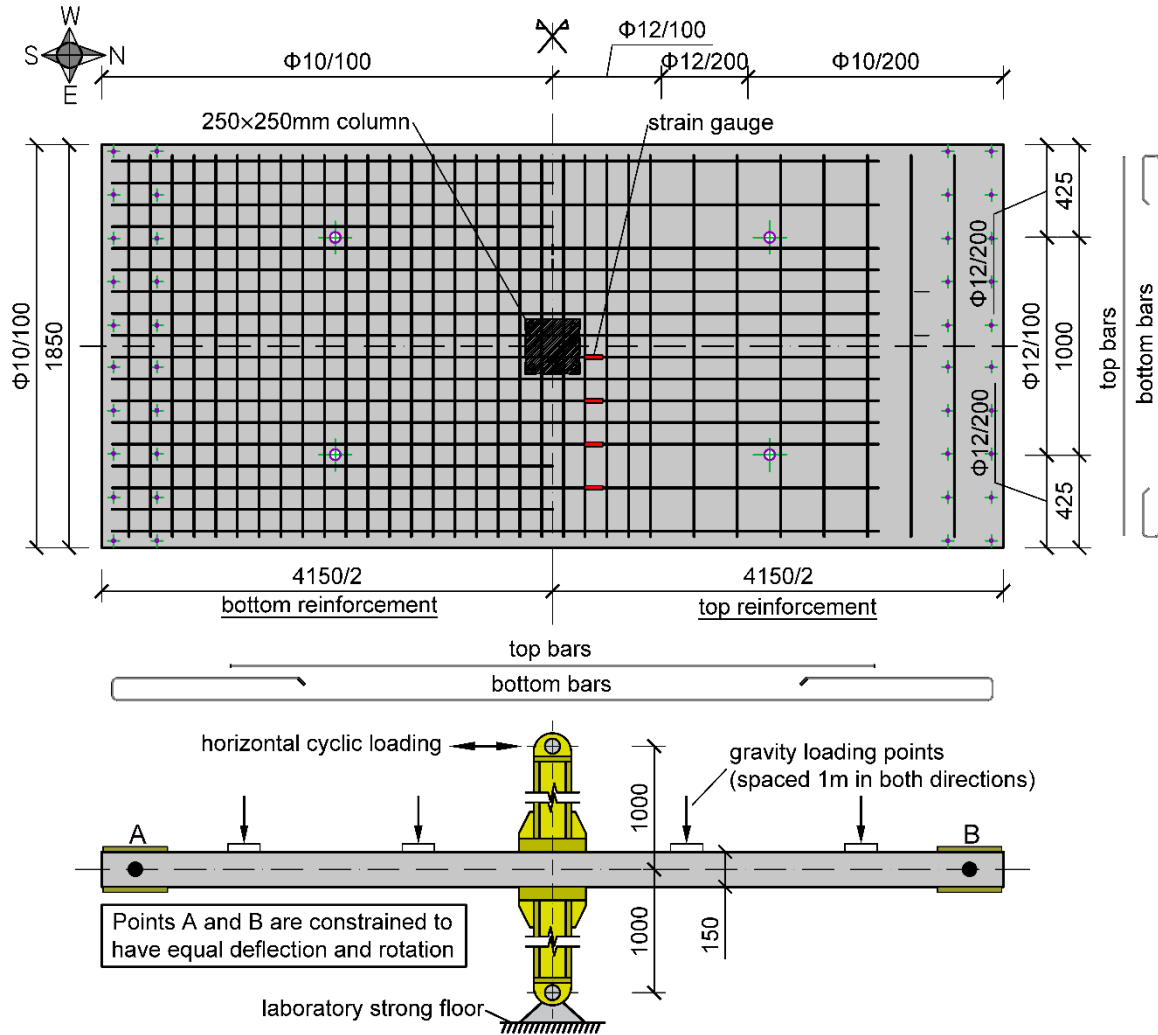


Fig. 1–Overall geometry and reinforcement of the specimens (units: mm).

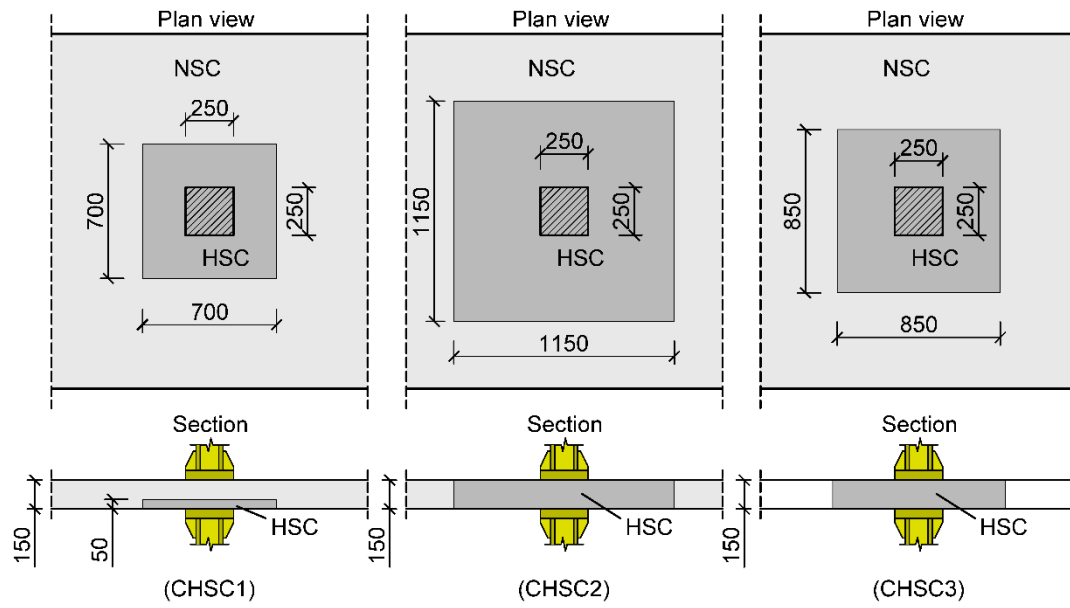


Fig. 2–Geometry of the HSC region in specimens (units: mm).



Fig. 3–Production of the specimens.

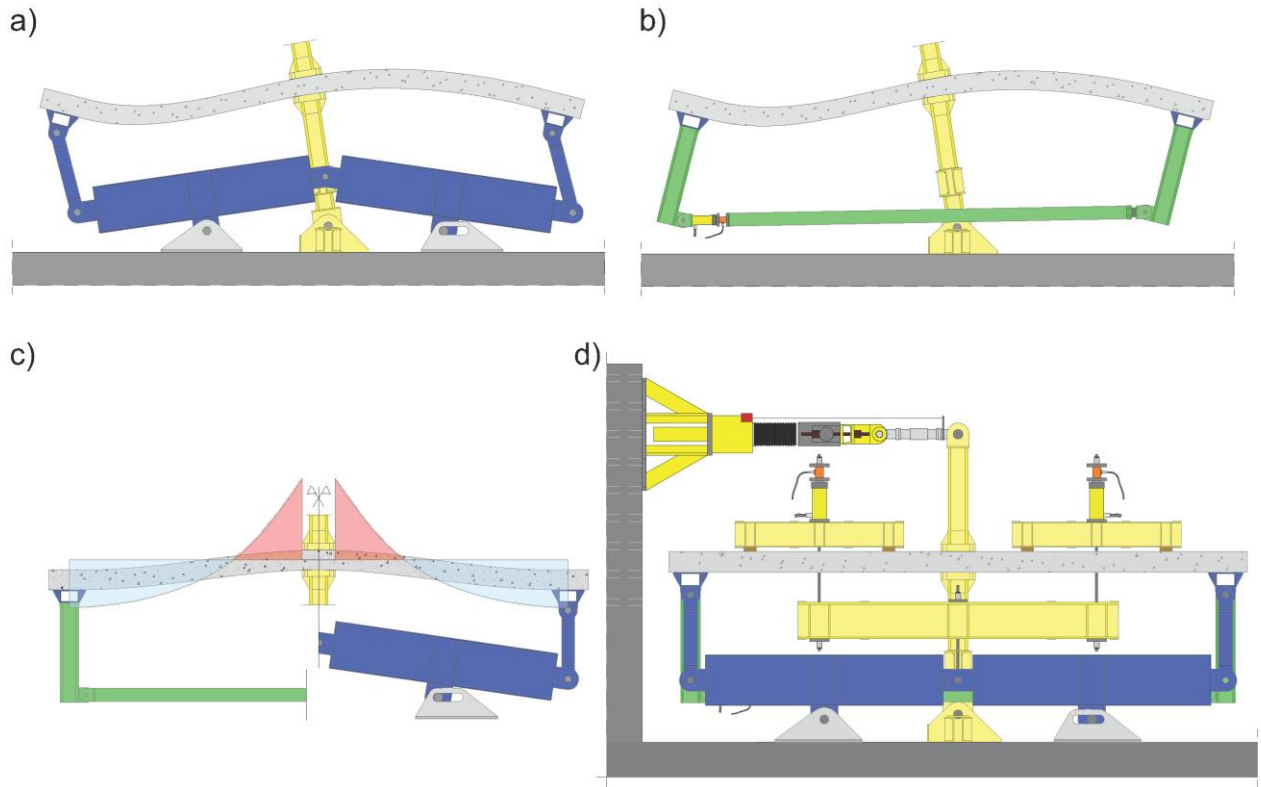


Fig. 4–Test setup; a) vertical displacement and shear force compatibilization system under slab's vertical and horizontal deformation; b) rotation and bending moment compatibilization system under slab's vertical and horizontal deformation; c) bending moments diagram under gravity loading; d) general view.

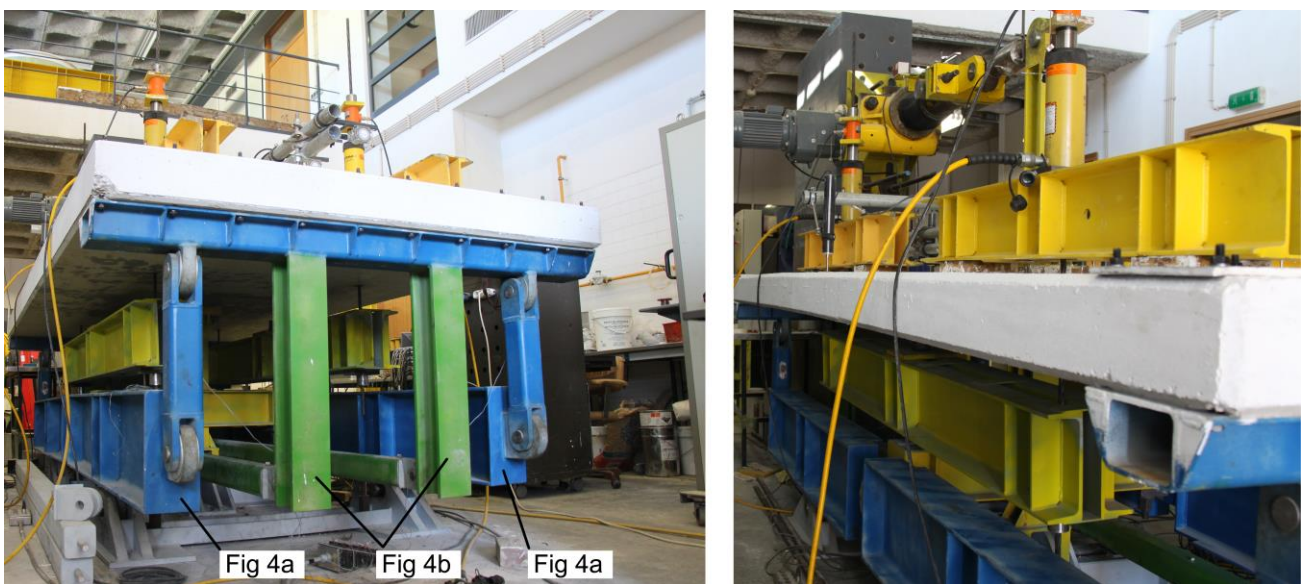


Fig. 5–Photos of the test setup.

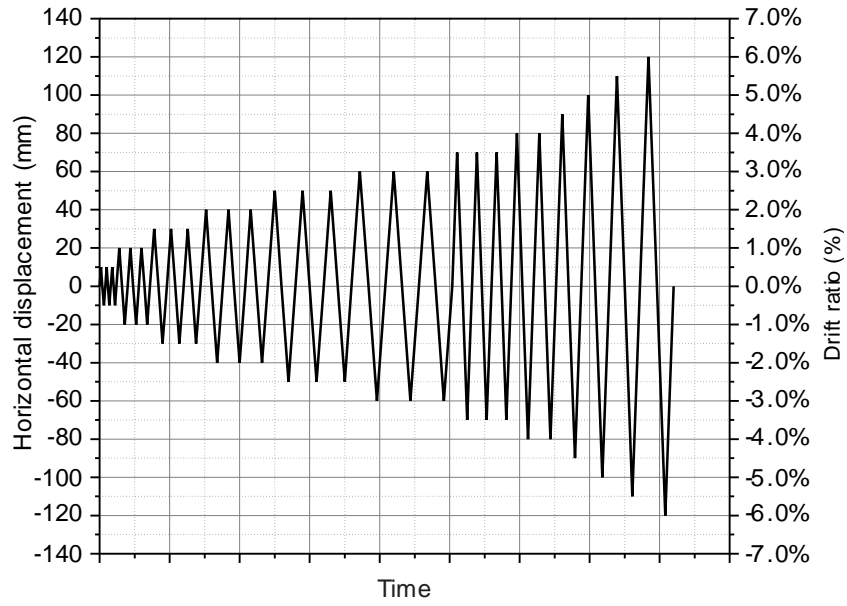


Fig. 6–Horizontal loading protocol.

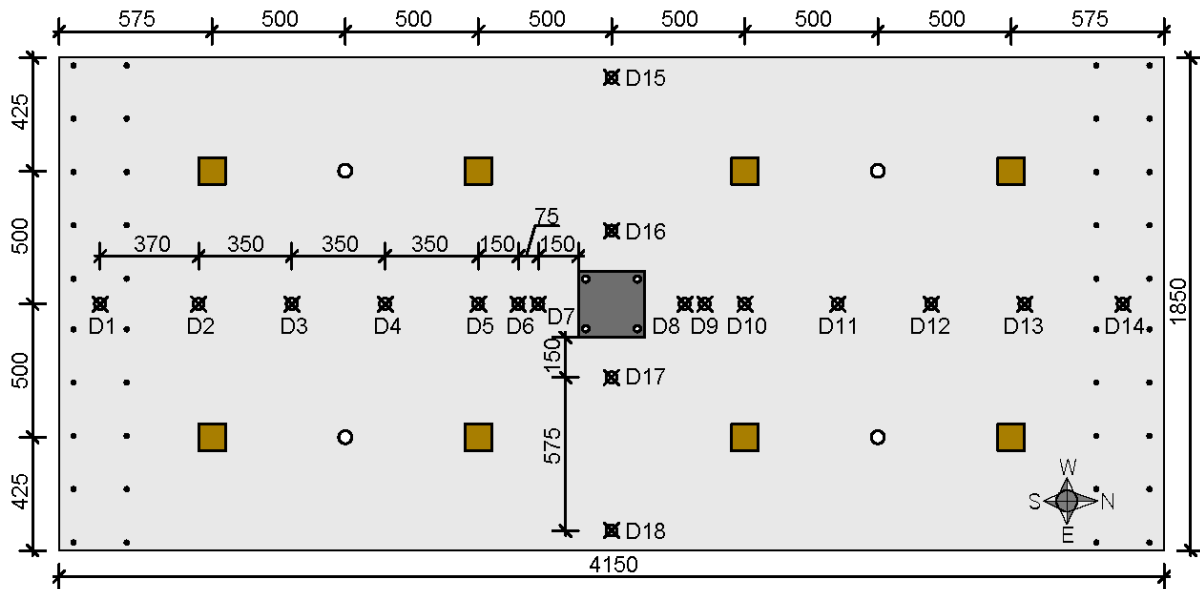


Fig. 7–Instrumentation and gravity load application points.

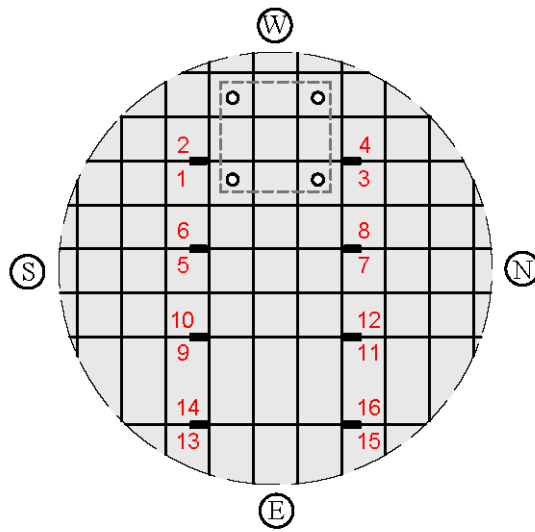


Fig. 8–Instrumentation of top flexural reinforcement bars.

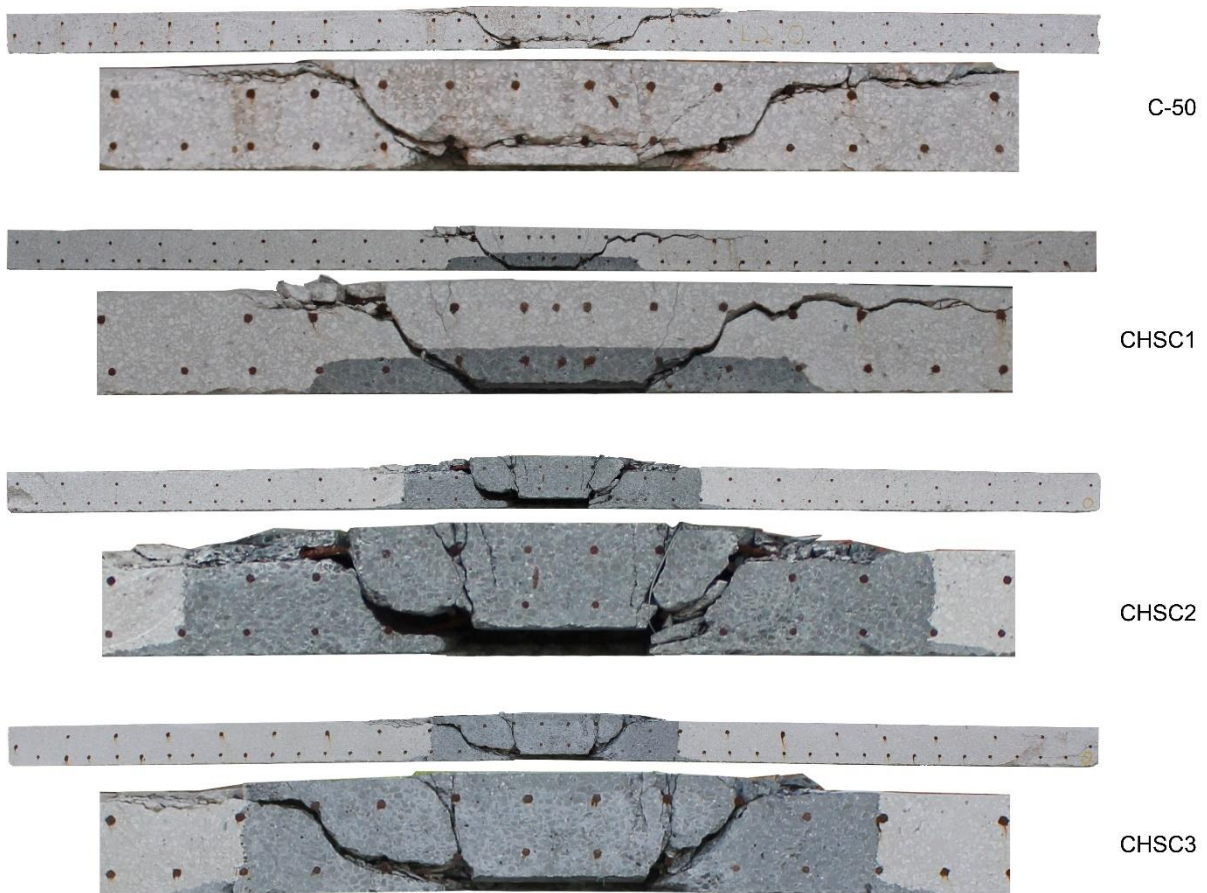


Fig. 9–Saw-cuts of the specimens.

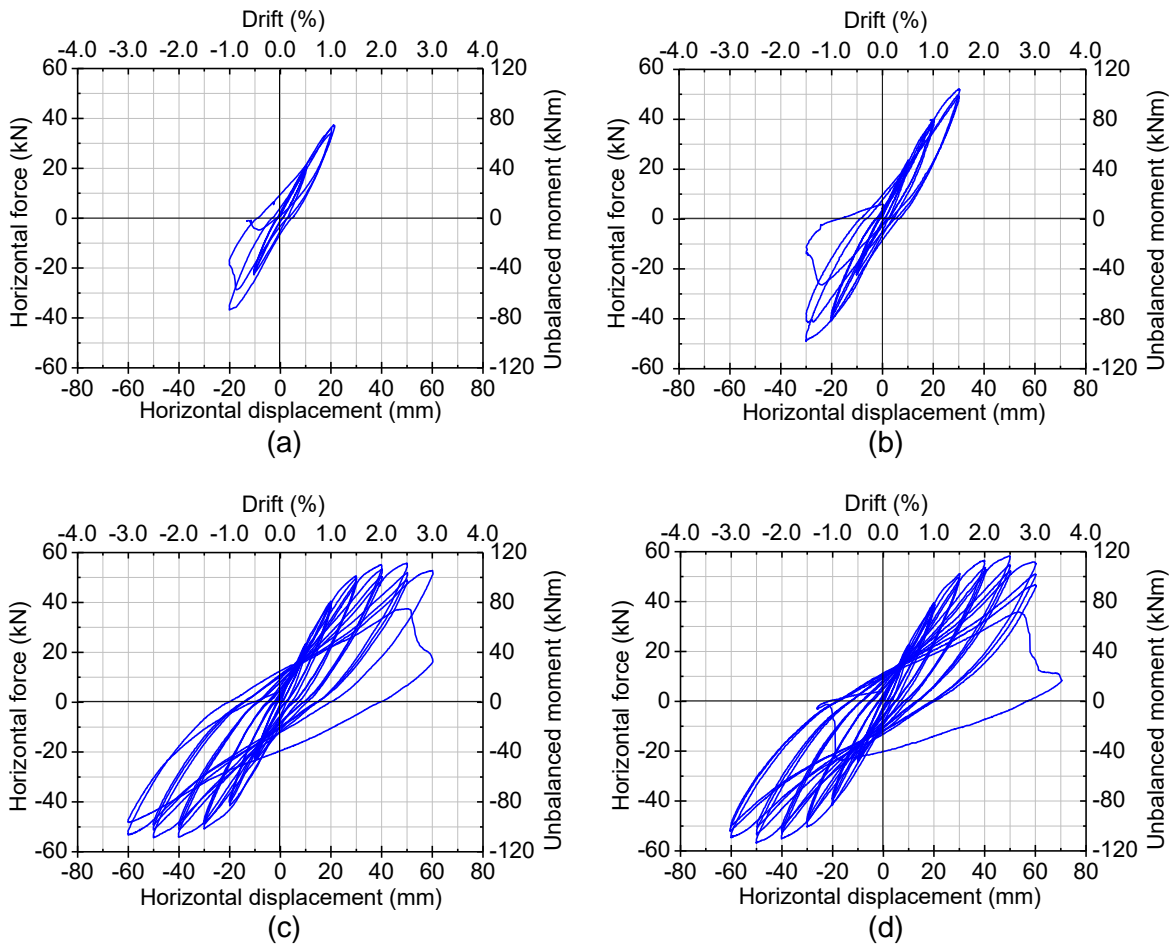


Fig. 10—Force—displacement relationship for specimen: a) C-50; b) CHSC1; c) CHSC2 and d) CHSC3.

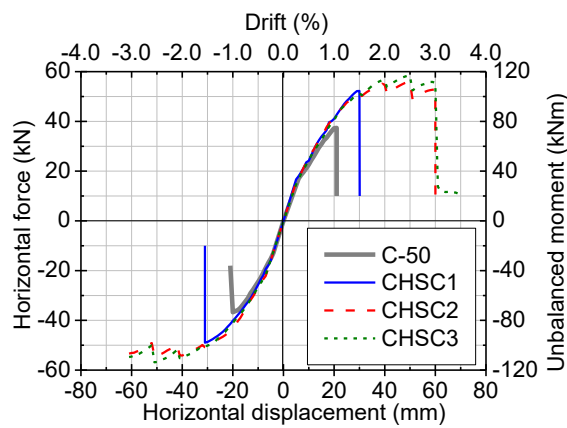


Fig. 11—Envelope force—displacement curves for all specimens.

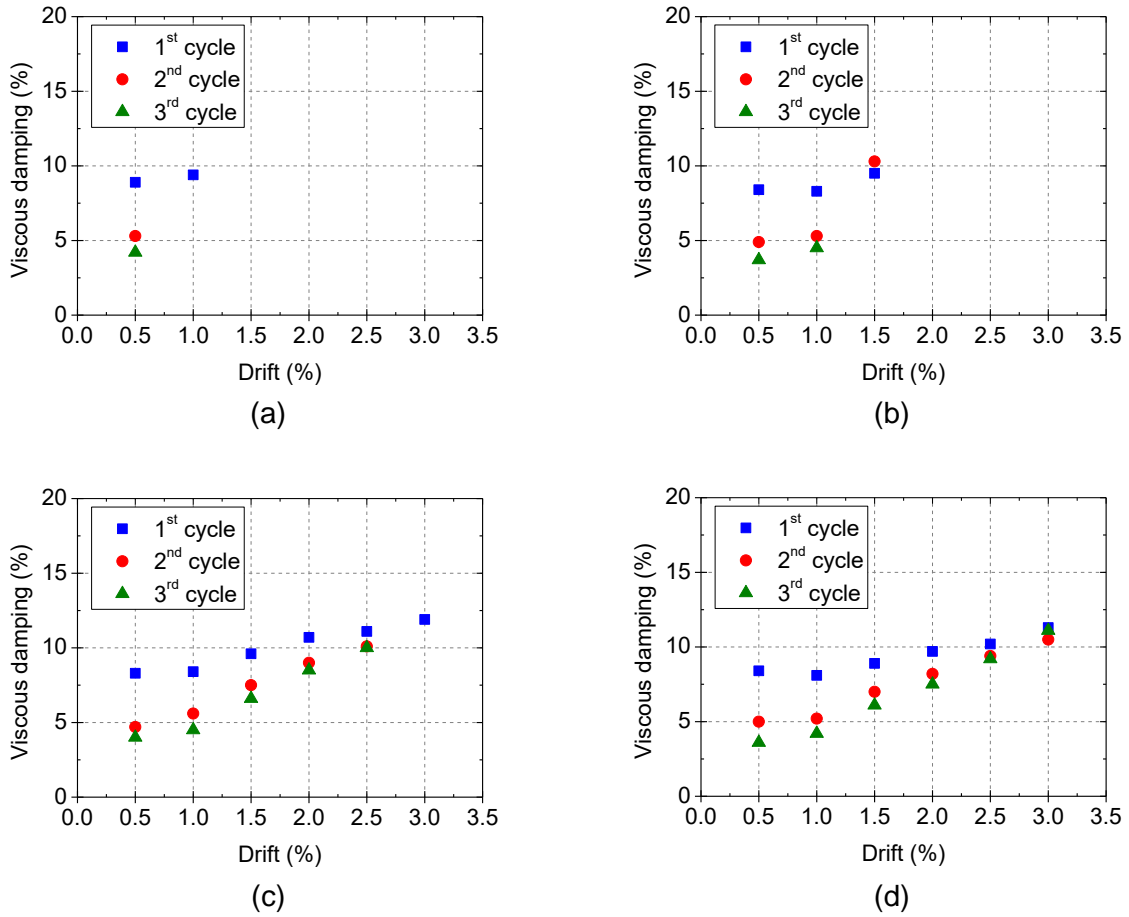


Fig. 12—Equivalent viscous damping; a) C-50; b) CHSC1; c) CHSC2; d) CHSC3.

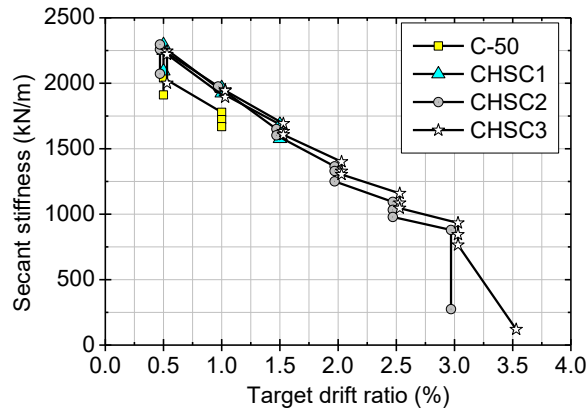


Fig. 13—Stiffness degradation

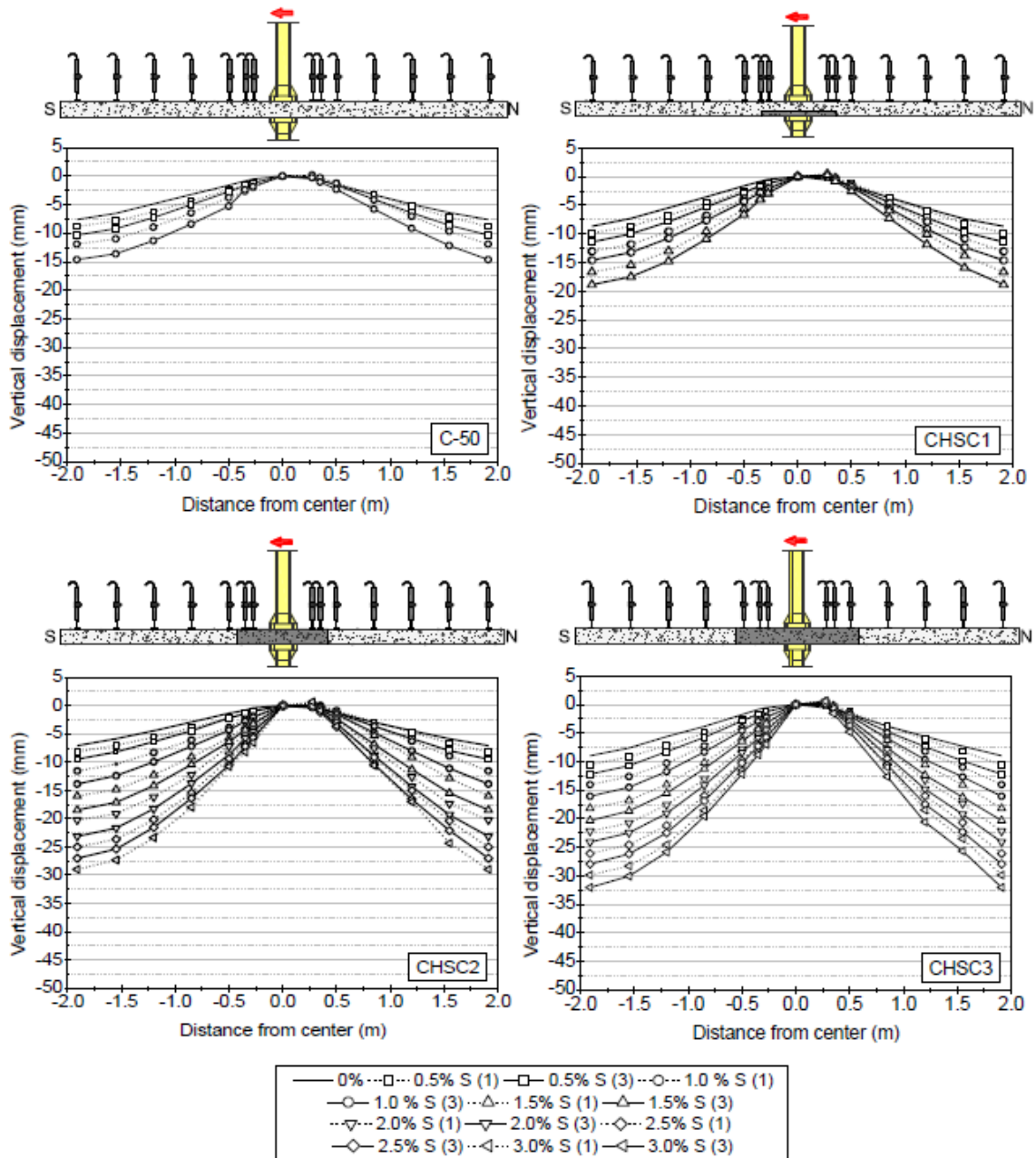


Fig. 14–Deflection profiles in the longitudinal (North-South) direction.

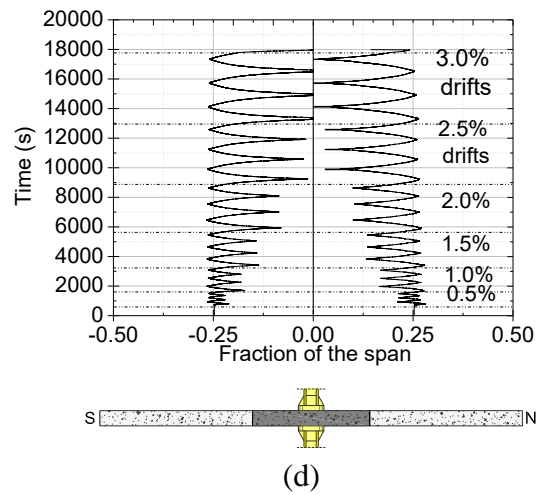
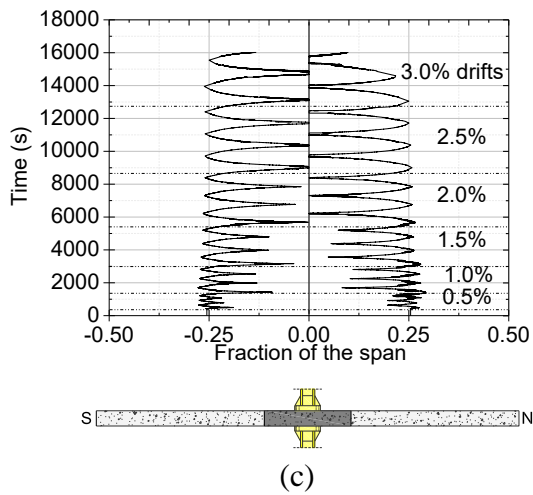
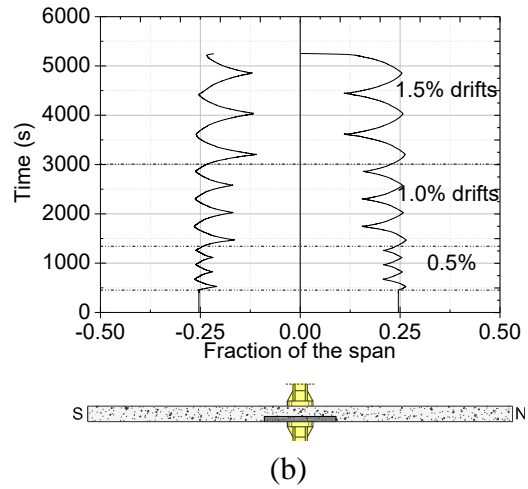
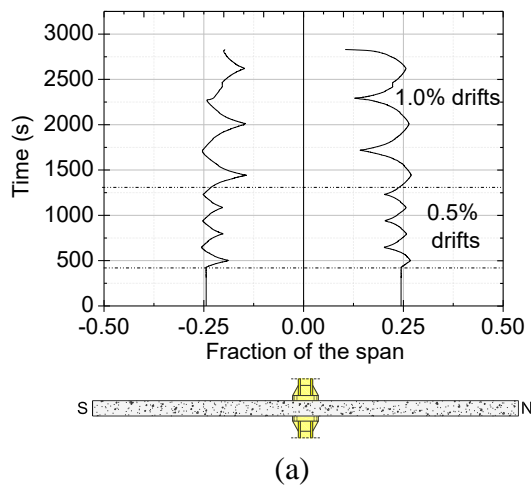


Fig. 15—Location of the inflection point in the longitudinal direction of the specimens; a) C-50; b) CHSC1; c) CHSC2; d) CHSC3.

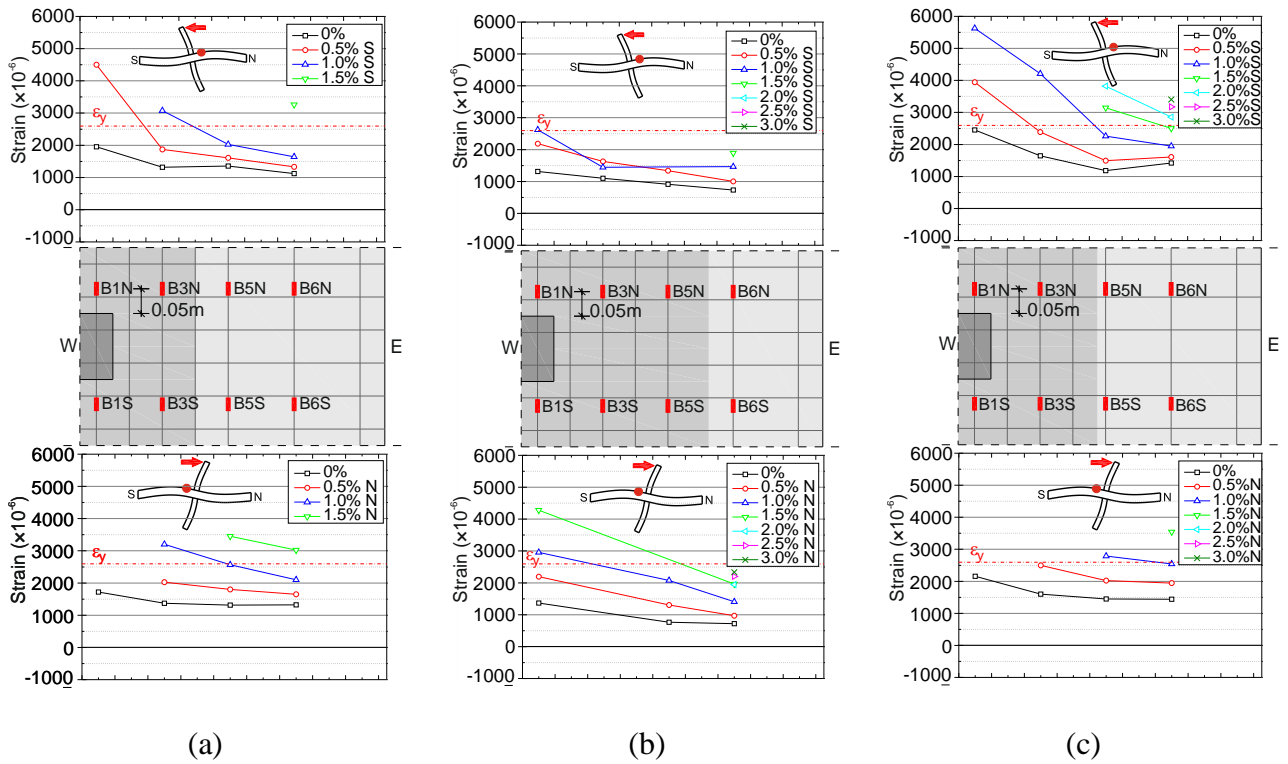


Fig. 16–Strain gauge readings in the flexural reinforcement; a) CHSC1; b) CHSC2; c)

CHSC3.